This is a post-peer-review, pre-copyedit version of an article published in [Water, Air, & Soil Pollution]. The final authenticated version is available online at: http://dx.doi.org/[10.1007/s11270-021-05052-z]"

Visibility graph analysis of particle size distribution during flocculation for water treatment

Kamila Jessie Sammarro Silva[1], Larissa Lopes Lima[2], Gustavo Santos Nunes[1], Lyda Patricia Sabogal-Paz[1]*

[1]São Carlos School of Engineering, University of São Paulo, Department of Hydraulics and Sanitation, Avenida Trabalhador São-carlense 400. São Carlos, São Paulo. Zip code: 13566-590. Brazil.

[2]Federal Center for Technological Education of Minas Gerais, Postgraduate Program in Mathematical and Computational Modeling. Av. Amazonas, 7675. Belo Horizonte, MG. Zip code: 30510-000. Brazil.

kamilajessie@usp.br / larissalopeslima@yahoo.com.br / gsnunes94@gmail.com / lysaboga@sc.usp.br*

*corresponding author

Orcid ID

0000-0002-6881-4217

0000-0003-2535-828X

0000-0002-3665-6138

0000-0003-2753-3248

Abstract: Water and wastewater physicochemical treatments often rely on coagulation and flocculation to generate aggregates adequate for separation. Floc development may be assessed by particle size distribution (PSD) using dynamic light scattering techniques (DLS) available in commercial equipment. The DLS output data, however, often presents high variability, which may hinder comparisons of the aggregation time series for different conditions. The Visibility Graph (VG), a novel approach to be applied within the sanitation context, may be an alternative to disclose properties of these highly oscillatory monitoring results. In this study, after defining ideal shear rates and mixing times for the treatability of high turbidity test water, we monitored PSD after coagulation using metallic salts (ferric chloride and ferric sulfate) and a natural coagulant (*Opuntia cochenillifera*). PSD data was converted to visibility networks and measurements were obtained to describe these time series by the VG technique. Although no series patterns were found, the VG approach shed some light onto the PSD through time, but no inferences were scaled to the treatability aspect. The limitations for the VG method in this study are mainly due to the small time series, thus we endorse that visibility network analysis may be a promising technique within the environmental and sanitation context.

Keywords: Time-series analysis; coagulation; *Opuntia cochenillifera*; ferric sulfate; ferric chloride

Declarations

Funding: The Global Challenges Research Fund (GCRF) UK Research and Innovation (SAFEWATER; EPSRC Grant Reference EP/P032427/1) supported this work. The Coordination for the Improvement of Higher Education Personnel (CAPES-PROEX – Financial code 001) granted Kamila Jessie Sammarro Silva with a PhD scholarship. Minas Gerais Research Funding Foundation (FAPEMIG) granted Larissa Lopes Lima with a PhD scholarship. The National Council for Scientific and Technological Development (CNPQ) granted Gustavo Santos Nunes with a Master scholarship.

Conflict of interest: No potential conflict of interest was reported by the authors.

Introduction

Coagulation and flocculation are important phenomena in water and wastewater treatment (Ching et al. 1994; Bratby 2016) that depend upon the interaction between factors such as size, shape, density, source and composition of suspended particles (Saritha et al. 2017). These are matrix-dependent and must be considered, particularly because, within the sanitation field, matrices can be as different in characteristics as in source waters (Soros et al. 2019), industrial wastewaters (Land et al. 2020), food-based and agro-industrial wastewater (Tonhato Junior et al. 2019; Sacchi et al. 2020), dam water (El Foulani et al. 2020), landfill leachate (Ghafari et al. 2009; Adlan et al. 2011), among others. The effectiveness of a physicochemical treatment system relies directly on the performance of the integrated coagulation-flocculation process (de Oliveira et al. 2016), which is also largely affected by the coagulant properties. These can be organic, inorganic or composites and therefore perform within different coagulation mechanisms (Zhu et al. 2011).

Among chemical coagulants, the most common can be divided in two general categories: those based on aluminum (as aluminum sulfate, aluminum chloride, sodium aluminate, aluminum chlorohydrate, etc.) and those based on iron (as ferric sulfate, ferrous sulfate, ferric chloride, polyferric sulfate and others) (Bratby 2016). These two groups have been used as coagulants in water and wastewater treatment for many decades and they can generate positively charged hydrolysis products that neutralize the negative charge of colloidal impurities (5×10^{-3} to 1 μm), leading to coagulation. (Gregory and Dupont 2001). Natural coagulants, particularly vegetal-based ones, have also been used for coagulation throughout the years (Muruganandam et al. 2017). Some natural polymers have stood out as those obtained from *Moringa oleifera* seeds (Miller et al. 2008; Adesina et al. 2019), *Aloe vera* leaves (Muruganandam et al. 2017) and by cacti such as *Opuntia* spp. (Miller et al. 2008; Bratby 2016; Souza Freitas and Sabogal-Paz 2019).

After colloidal destabilization, flocculation takes place for particle aggregation by means of shear-induced collision and orthokinetic forces, leading to flocs, which will vary in characteristics as a function of shear rate and time (Moruzzi et al. 2017). An indirect measure for optical monitoring of aggregates is the determination of particle size by light scattering, which is a very well established technique for which commercial devices are available (Gregory 2009). For given operational conditions during flocculation, a dynamic steady-state is expected for PSD over time (Jarvis et al. 2005). PSD data, however, may present oscillations when carried out by destructive sampling methods. Microflocs can be highly irregular and porous, which leads their scattering patterns to differ from ideal solid spheres of the same material in light scattering equipment (Jarvis et al. 2005). Light scattering is therefore considered an interesting option to monitor qualitative, rather than absolute characteristics of aggregates during flocculation (Farrow and Warren 1993), but it opens a field of investigation for other time series analysis approaches.

In scientific investigation, when there is no clear correlation among data using conventional statistics, one of the possibilities is to resort to alternative techniques, as in Visibility Graphs (VG), that may reveal evolutionary behaviors, not elucidated by time-series analysis (Lacasa et al. 2008). The visibility-network analysis, may therefore be a tool to analyze temporal features of the mapped series without compromising their structure (Lacasa et al. 2009; Iacobello et al. 2018). The synthetic networks can disclose properties of the time series, for example: periodic, random, or fractal series can become regular, random, and scale-free networks, respectively (Yang et al. 2009). VG applications have been described in health sciences (Ahmadlou et al. 2010; Jiang et al. 2013; Supriya et al. 2016; Gao et al. 2016, 2017; Xiong et al. 2019), economics (Wang et al. 2012; Long 2013; Jiang et al. 2016; Gonçalves et al. 2019), physics (Liu et al. 2010; Gonçalves et al. 2016; Iacobello et al. 2018), geosciences (Donner and Donges 2012; Telesca and Lovallo 2012), among other research fields. Sanitation approaches, however, have not been further explored.

In this scene, the aim of this study was to provide a novel attempt of using VG to explore the temporal evolution of PSD during floc formation when coagulation was performed with metallic coagulants (ferric chloride and ferric sulfate) and a natural coagulant (*Opuntia cochenillifera*) in test water.

Materials and methods

Test water

The test water simulated a water quality of both high color and turbidity, aiming at an average of 100 NTU and 30 UH of true color. It was prepared using non-chlorinated natural water from a well located at São Carlos School of Engineering (SCSE/USP, São Carlos, Brazil), into which kaolinite (Sigma-Aldrich®) and humic acid (Sigma-Aldrich®) were added. Initial quality was tested prior to every treatability test, as well as the mixture optimization experiments and PSD assays.

Coagulant preparation

Ferric chloride and ferric sulfate (both purchased from Sigma-Aldrich®) stock solutions (20 g L^{-1}) were prepared prior to the experiments and proper dilutions were carried out for the jartest runs. *Opuntia cochenillifera (O. cochenillifera)* was chosen as natural coagulant, considering its efficacy in treating high turbidity water (Miller et al. 2008; Shilpa et al. 2012, Souza Freitas and Sabogal-Paz, 2019). Its pads were collected in the municipality of São Carlos (SP, Brazil) and had their thorns removed and cladodes rinsed in tap water. Afterwards, they were cut in one-centimeter strips. The extract applied in coagulation was a powder prepared according to (Miller et al. 2008; Shilpa et al. 2012). The procedure, in short, consisted in drying approximately 0.5 kg of freshly prepared cacti at 60 ºC for 24 hours. Dry *O. cochenillifera* was then grounded and sifted to a maximum of 300 µm average grain size. Images of the natural coagulant preparation are provided in the supplementary material.

Jar test

Preliminary treatability tests were run for each coagulant in order to allow selecting the best conditions in terms of pH and dose, which were evaluated for turbidity removal efficiency. pH was adjusted by either sodium hydroxide or sulfuric acid (both purchased from Sigma-Aldrich®) immediately before the jar tests. Metallic coagulants were tested at fixed conditions of 1,000 s^{-1} velocity gradient for 10 s during coagulation and 20 s^{-1} during a 30-minute flocculation. Settling velocity was fixed at 1.5 cm min^{-1}. As for *O. cochenillifera*, the parameters for the preliminary treatability assays were 250 s^{-1} for 60 s during rapid mix and 25 s^{-1} for 20 minutes during flocculation (Miller et al. 2008). Settling velocity for the natural coagulant was fixed at 0.25 cm min^{-1}.

These chemical parameters, defined for each coagulant, led to a second treatability run, which was carried out in triplicate for each operational condition, using the one-factor-at-a-time experimentation method (Frey et al. 2003). The operational variables under test (Fig. 1) were: rapid mixing shear rate (coagulation velocity gradient, coagulation time), and slow mixing shear rate (flocculation velocity gradient, flocculation time). Settling velocity was fixed at 1.5 cm min^{-1} for ferric chloride and ferric sulfate and at 0.25 cm min^{-1} for treatments with *O. cochenillifera*. The operational conditions that maximized turbidity removals were selected for the PSD assessment.

Fig. 1 Schematic of the experimental design for coagulation and flocculation shear rates for optimizing treatability

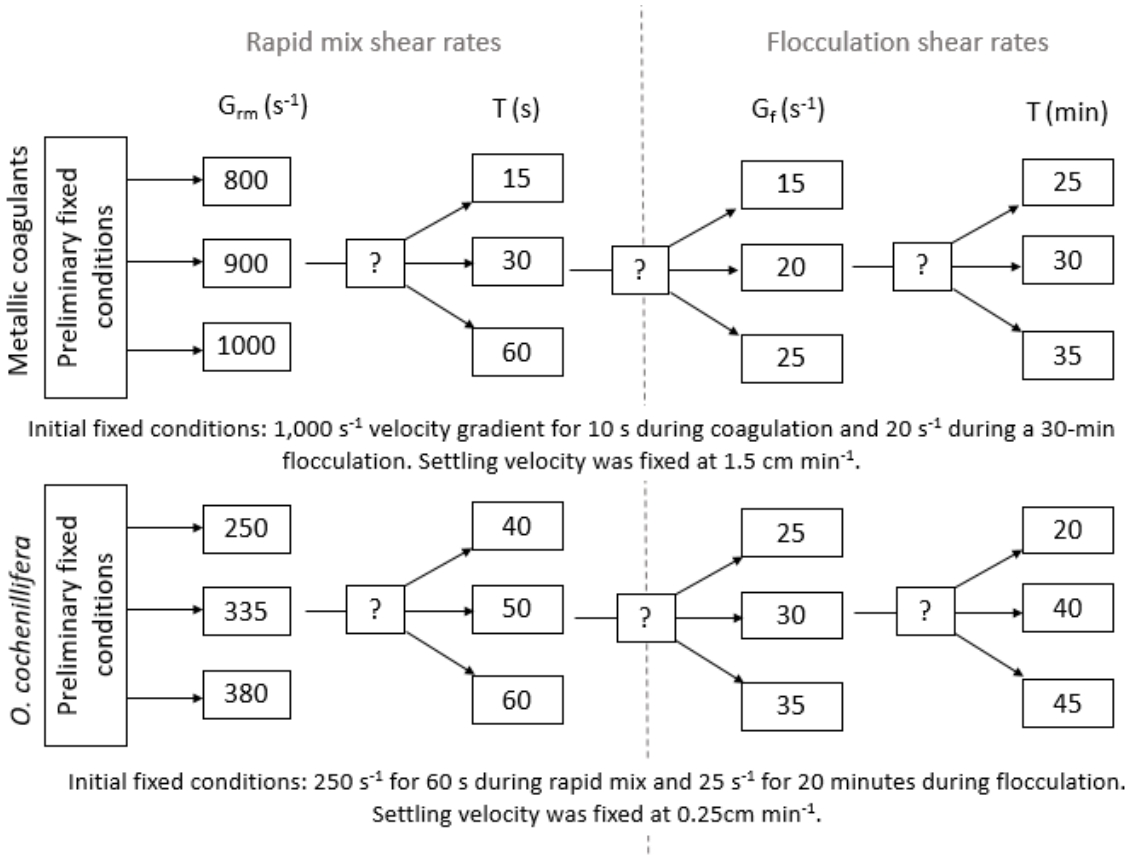

Note: Gmr = velocity gradient during rapid mix; Gf = velocity gradient during flocculation; T = time

Particle size distribution

Floc aggregation was analyzed by PSD, by measuring micro-flocs z-average hydrodynamic diameters using a Zetasizer Nano ZS90 (Malvern Instruments Ltd.). The equipment operates by dynamic light scattering (DLS), and the detection range provided measurement from 0.3 nm (diameter) to 5 microns using 90 degree scattering optics.

Samples were collected from the jars during flocculation in two-minute time-steps for 34 minutes. In order to provide a broader view of the flocculation progress, flocs were monitored during a period that exceeded the optimized slow mixing time for some coagulants, previously assessed. Macroflocs were not captured for DLS analysis, as they do not fit particle sizes and suspension ionic strength for the

Smoluchowski approximation model (Elimelech et al. 1998), applied in the equipment's standard operational procedure.

Data analysis

All of the time series were considered to have started after minute two, as time zero referred to raw water, without any coagulants, which could have interfered in PSD and mass content. Univariate statistical analysis of the data series was performed using PAST software (Hammer et al. 2001). The data sets were first tested for normality ($\alpha = 0.05$) by Shapiro-Wilk test and log transformations or non-parametric analyses were carried out for situations in which data was not normally distributed.

The Visibility Graph (VG) technique was applied for an attempt of complementing data analysis. In a VG, a line is drawn between two data points. If the line does not cross any other points within the series, the two referring points are corresponding, i. e. there is visibility between them. Following a VG procedure proposed by Lacasa et al. (2008), the mathematical formulation may be given by two arbitrary values (x_a, y_a) and (x_b, y_b). They present visibility (and are connected) if any other value (x_c, y_c) located between them fulfills the condition $y_c < y_b + (y_a - y_b)\frac{(x_b - x_c)}{(x_b - x_a)}$, considering $x_a < x_c < x_b$. Dots are connected if there is a link between them. These linked dots become the nodes of the network, and the edges are the connection, therefore creating a VG data series graph, so the network is built.

Using the graph data, three measures were calculated: degree, betweenness centrality and closeness centrality (Sayama 2015). Degree is the number of connections from a node, whereas betweenness centrality measures the extent to which a vertex is present in paths between other vertices.

Then, the betweenness centrality (g) of a node v is given by:

$$g(v) = \sum_{s \neq v \neq t} \frac{\sigma_{st}(v)}{\sigma_{st}} \qquad \text{Equation (1)}$$

Where σ_{st} is the total number of shortest paths from node *s* to *t* and $\sigma_{st}(v)$ is the number of those paths that pass through *v*. We also performed a normalization, which is given by dividing Equation 1 by $(N-1)(N-2)/2$, since the graph is undirected. N is the number of nodes (vertices) of the graph.

Closeness centrality (*C*) measures the mean distance from a vertex to other vertices and is given by:

$$C(v) = \frac{N-1}{\sum_u d(v,u)} \qquad \text{Equation (2)}$$

Where *d(v,u)* is the distance between vertices *v* and *u*.

Results and discussion

Treatability assays

Jartest runs for chemical parameters suggested 20 mg L^{-1} as optimal dosage for ferric chloride at pH 6, leading to 99.7 % turbidity removal (0.39 NTU residual) and a 97.6% color reduction (final apparent color value of 3.7 HU). As for ferric sulfate, 30 mg L^{-1} was chosen at a coagulation pH of 6, which lead to a final turbidity of 0.36 NTU and apparent color of 6.1 HU (99.7 % and 95.9 % removals, respectively). For the mixture optimization tests, 30 mg L^{-1} of dry *O. cochenillifera* dosing was selected at 10 pH. This condition led to a reminiscent water turbidity of 3.66 NTU and the color to 31.2 HU, referring to 96.8 % and 79.0 % respective removals.

Fig. 2 displays stepwise optimal results for mixture shear rates selection for the treatment with ferric chloride, in terms of final turbidity. Similarly, Fig. 3 and Fig. 4 refer to such operational conditions partial results for ferric sulfate and *O. cochenillifera* as coagulants, respectively. Table 1 presents the operational conditions selected for PSD assessment for each coagulant under study.

Fig. 2 Final turbidity obtained by coagulation-flocculation assays using ferric chloride for one-factor-at-a-time optimization varying (a) rapid mixture velocity gradient; (b) rapid mixture time; (c) slow mixture velocity gradient; (b) slow mixture time

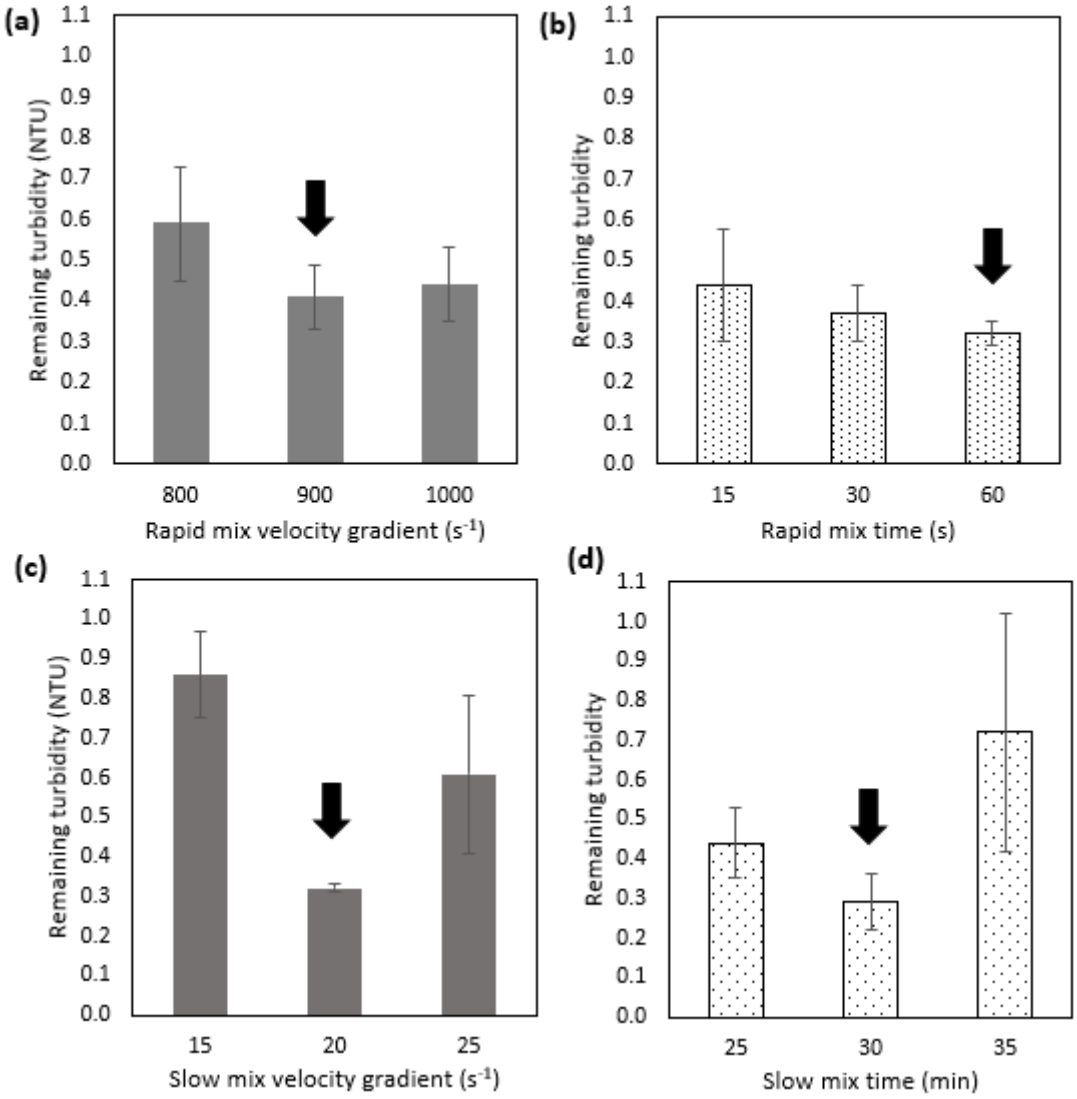

Note: Sedimentation velocity fixed at 1.5 cm min^{-1}. Black arrows point to selected conditions.

Fig. 3 Final turbidity obtained by coagulation-flocculation assays using ferric sulfate for one-factor-at-a-time optimization varying (a) rapid mixture velocity gradient; (b) rapid mixture time; (c) slow mixture velocity gradient; (d) slow mixture time

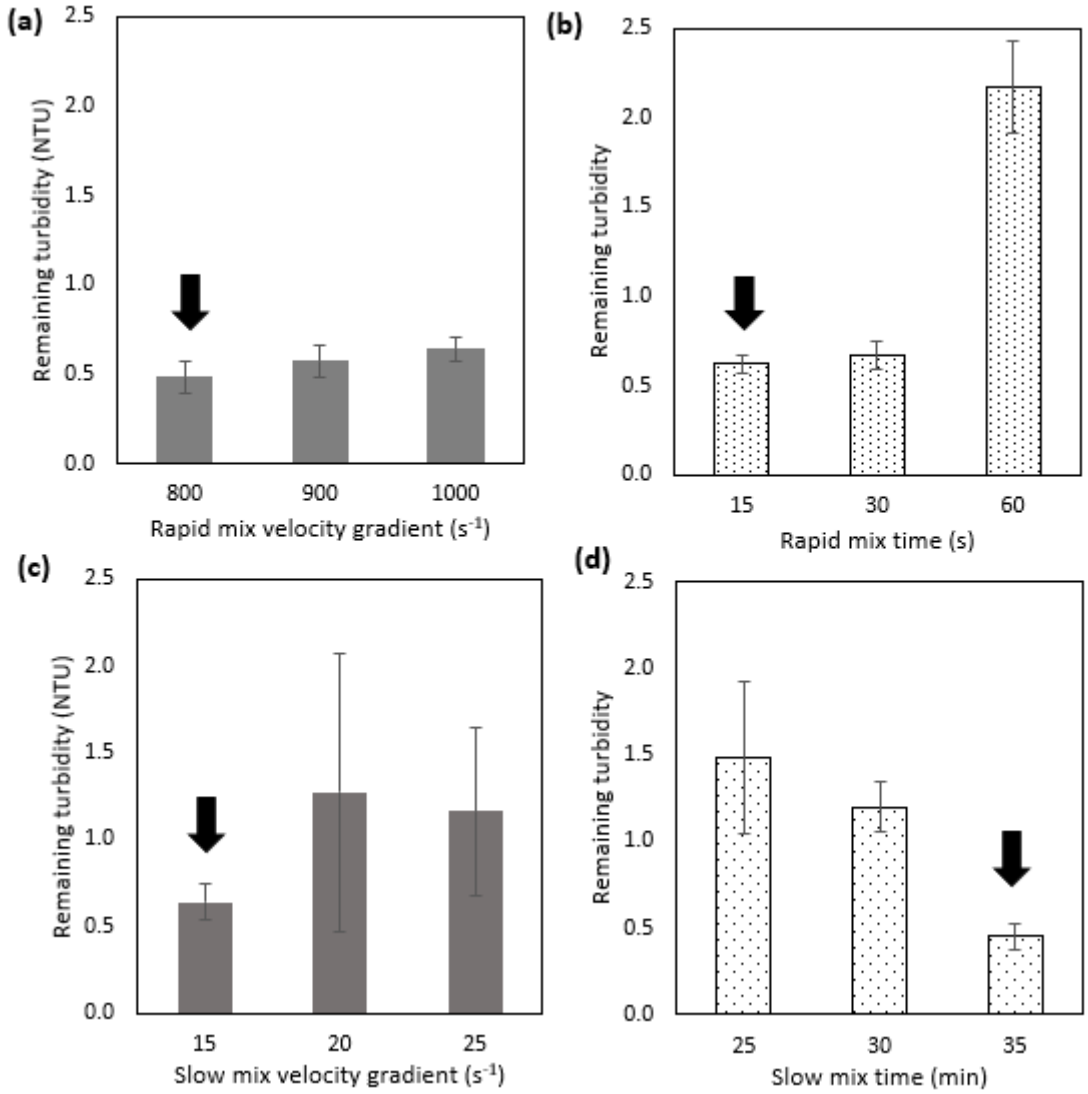

Note: Sedimentation velocity fixed at 1.5 cm min^{-1}. Black arrows point to selected conditions.

Fig.4 Final turbidity obtained by coagulation-flocculation assays using *O. cochenillifera* for one-factor-at-a-time optimization varying (a) rapid mixture velocity gradient; (b) rapid mixture time; (c) slow mixture velocity gradient; (d) slow mixture time

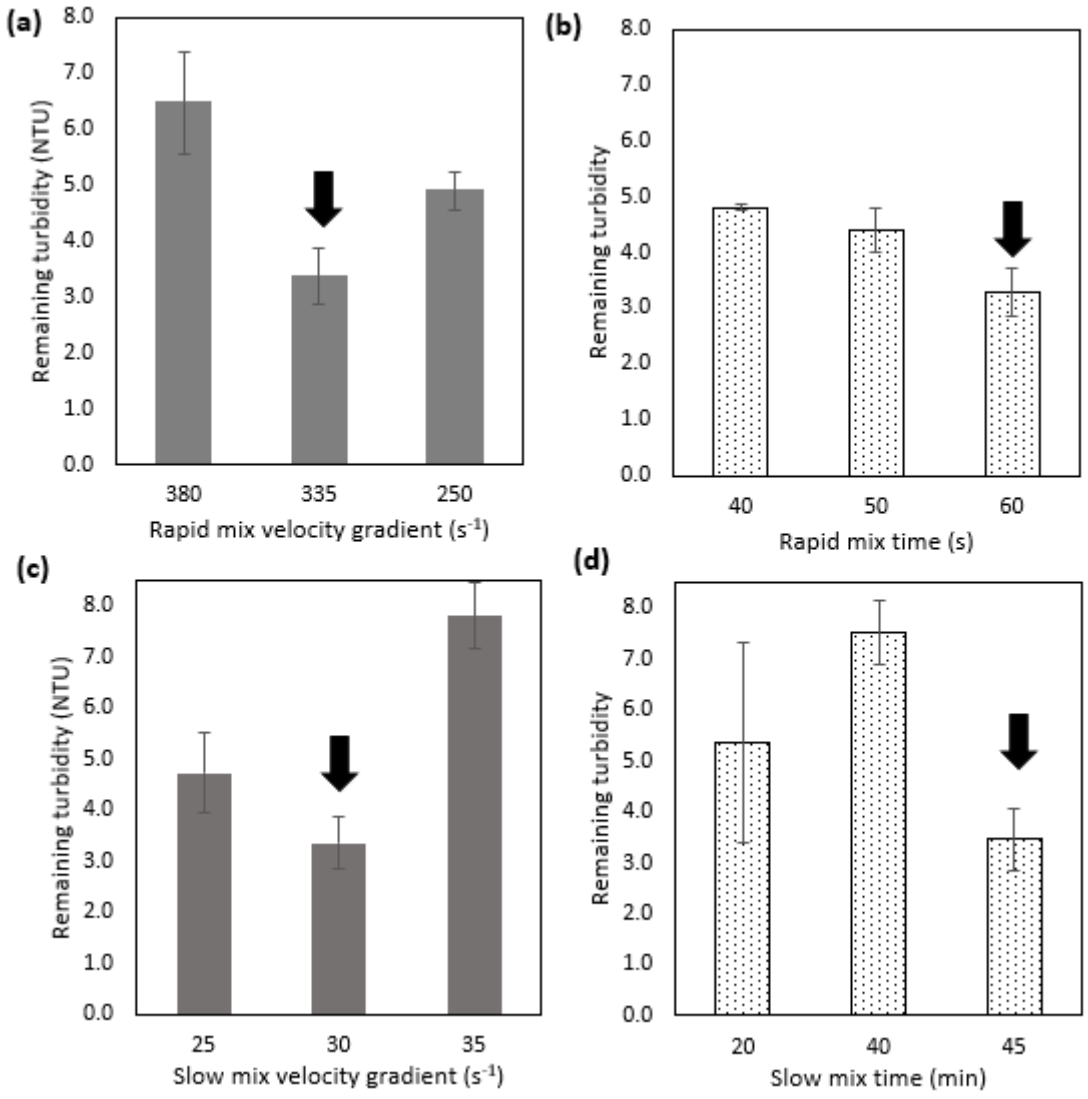

Note: Sedimentation velocity fixed at 0.25 cm min^{-1}. Black arrows point to selected conditions.

Table 1 – Optimal operational parameters selected for treatability assays performed for particle size distribution assessment during flocculation

Coagulant	Dose (mg L^{-1})	Initial pH	Rapid mix		Flocculation		Color removal efficiency (%)	Turbidity removal efficiency (%)
			Gradient (s^{-1})	Time (s)	Gradient (s^{-1})	Time (min)		
Ferric chloride	20	7	900	60	20	30	88.3	99.4
Ferric sulfate	30	8	800	15	15	35	99.6	99.4
Opuntia cochenillifera	30	10	335	60	40	45	80.1	95.7

Average test water quality: 85 ± 14 NTU; 156.7 ± 12.4 uH; 25ºC. pH refers to average adjusted values applying sodium hydroxide. Particle size distribution of the treatment was monitored for 34 min for the metallic coagulants and 46 min for *O. cochenillifera*, which surpassed optimal flocculation time.

Visibility Graph for particle size distribution through time

PSD assessed through flocculation, displayed by Fig. 5 (a), presented high standard deviation for all of the coagulants under test, which ratifies an assumption of floc growth, or, at least, change during flocculation. As of data quality, samples were considered very polydisperse (PDI ~ 1), which may hinder DLS analysis. Ferric chloride and ferric sulfate mean Z-average size values were 10.327±8.722 µm and 14.316±8.626 µm, respectively. *O. cochenillifera* z-average size mean was 1.219±0.238 µm.

PSD data through time was not normally distributed for treatments with ferric chloride (Shapiro-Wilk normality test, $p = 0.0080$), nor *O. cochenillifera* ($p = 0.0056$), thus non-parametric univariate statistics was carried out. The Kruskal-Wallis test indicated there was significant difference between sample medians ($p < 0.0001$). Dunn's post-hoc test suggested such differences were present when comparing *O. cochenillifera* PSD data to both ferric chloride and ferric sulfate ($p < 0.0001$), whereas metallic coagulants did not present statistically significant differences themselves. In short, medians of the temporal distribution are statistically different between the metallic coagulants and the vegetal-based one, endorsing results from descriptive statistics and observational inferences from Fig. 5 (a).

Nevertheless, these conclusions do not provide any inferences on floc development through time, which was assessed by measurements of the obtained VGs. These are also shown in Fig. 5 (b, c, d).

Fig. 5 Particle size distribution during flocculation presented in (a) regular time series; visibility graphs for (b) ferric chloride; (c) ferric sulfate; (d) *Opuntia cochenillifera*

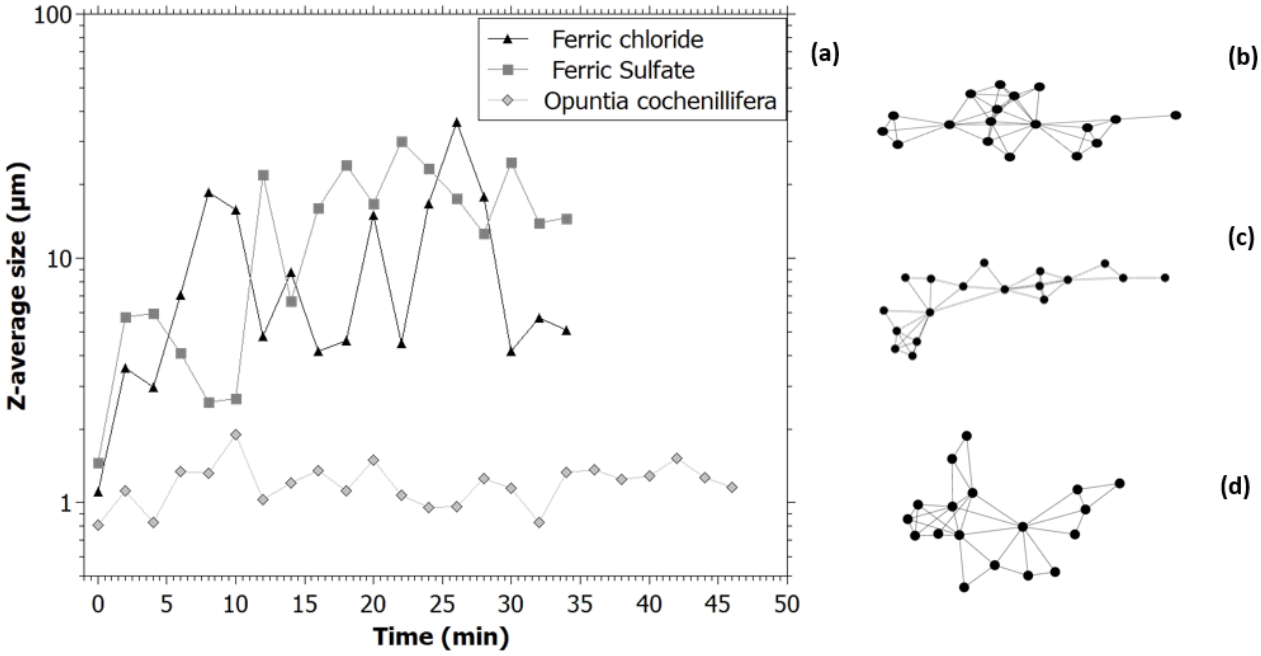

The node degree distribution (Fig. 6) reveals that flocculation with each of the three coagulants present most of the PSD nodes within a low degree range, whereas few nodes have higher degrees. As for ferric sulfate and *O. cochenillifera*, no node has a degree greater than 9. However, for ferric chloride, the node with the highest degree has 12 connections and, compared to the other coagulants, there are considerably fewer nodes with a degree of less than 3. This probably relates to the high oscillation between the mean particle size values for ferric chloride, when compared to the other coagulants, as displayed in Fig. 5 (a) and by descriptive statistics.

Node degrees were transformed to fit a normal distribution (checked by the Shapiro-Wilk test) and followed a one-way ANOVA test for equal means. Results indicated there were no statistically significant differences (p = 0.4212) for the degrees obtained throughout the treatments, in a matter of mean PSD. From a flocculation perspective, the homogeneity inferred by the degree in VG assessment

endorses that the operation is being carried out similarly for all of the coagulants under study, as particle size evolves within no statistically different number of connections for each node. As shown by the selection of operational parameters and their effects in turbidity removal efficiency, this is expected, considering the influence of the shear rates in floc formation. Nonetheless, the degree mean value does not point out the position in which such effects would occur. In addition, during flocculation in the metallic coagulant treatments, there was some mass loss due to particle settlement within the jars, which may have led to an effect in PSD readings, as some of the particles became unavailable. However, from a water treatment perspective, this relates to turbidity and color removals, which were to happen for all of the coagulants under test, considering an output of treated water. This conclusion was reiterated by confirming a null hypothesis of equal means in node degrees.

Fig. 6 Histogram of: (a) node degree; (b) betweenness centrality, and; (c) closeness centrality for the flocculation treatments

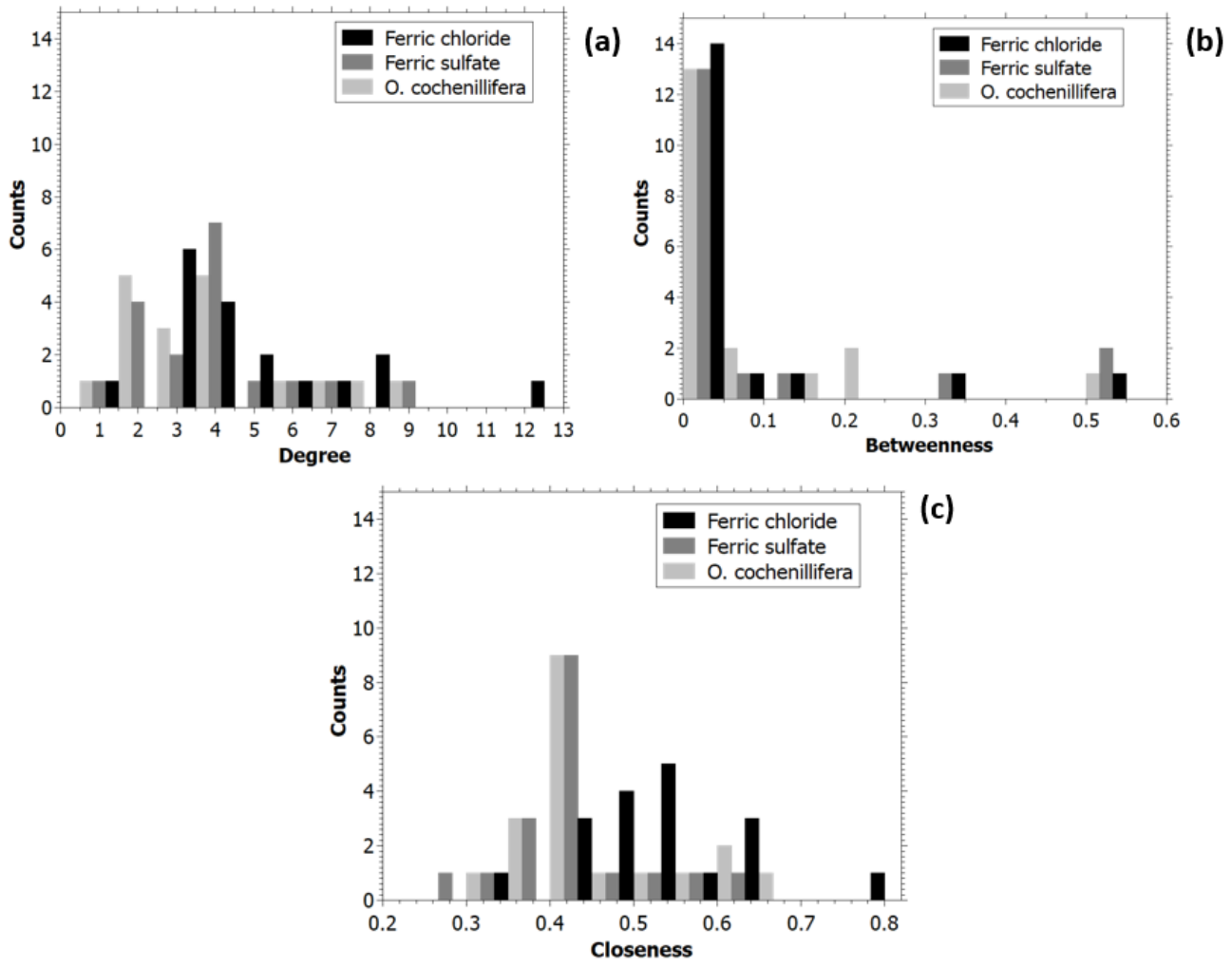

Betweenness centrality values were evaluated by non-parametric statistics, as they would not fit normal distributions. Kruskal-Wallis test for equal medians led to no significant differences (p = 0.7864). As of closeness centrality measurements, the data was logarithmically transformed, and one-way ANOVA suggested inequality of means. Tukey's post-hoc test indicated statistical differences between ferric chloride and ferric sulfate treatments (p = 0.0162), whereas no differences were found for the distance between nodes of *O. cochenillifera* when compared to the other treatments. This was an interesting element, as water clarification during flocculation, i. e. distinct macroflocs or even some particle settling, was not clear up to at least 15 minutes of slow mix for the natural coagulant. This

effect was visual for both ferric chloride and ferric sulfate at around 8 minutes of flocculation, suggesting similarities.

Measures derived from graphs displayed in Fig. 5 may provide an idea of the series behaviors. While ferric chloride could suggest a cyclical pattern for z-average size, oscillating between increase and decrease in particle size, ferric sulfate (after 15 minutes) and *O. cochenillifera* present less variability. Although there is no significant difference in degree, the closeness measure of ferric chloride is the one that presents a very different distribution from the others (Fig. 6). This may probably be caused by its particle size curve as a function of time, since closeness relates to the proximity of a node to the other nodes in the network.

Nevertheless, it must be noted that there are limitations in invasive PSD assessments, especially in sampling. As *O. cochenillifera* macroflocs present fibrous-like flocs (supplementary material), a common feature of natural-based coagulants (Miller et al. 2008; Subramonian et al. 2014), these were more easily avoided before subjecting samples to DLS. Here we infer this was compensated by early particle settlement for the metallic coagulants, leading to similar growth relationships between the nodes' network. Related to the effects on coagulation performance of iron-based coagulants (Wang et al. 2000), differences between closeness centralities may relate to the distribution of Fe species. The inherent and uncontrolled shifts in iron (III) ion presence (Chen et al. 2015) may affect the paths between nodes and different aggregates may have been captured throughout sampling.

It is worth noting that VG is a statistical physics technique, and usually attempts to elucidate patterns in large time series, common in financial analysis, for instance (Gonçalves et al. 2019). Here we have chosen a different perspective, applying VG to a small PSD time series, aiming to evaluate if there are any inferences that may be obtained from this approach. No behavior was generalized through the VG method, but results encourage future research applying VGs in floc size development. Here we suggest applying VG, for instance, in non-destructive floc growth assessment methods, as in imaging, which

should provide larger data sets and less variability in results than dynamic light scattering does for these test waters.

Conclusions

Shear rates and chemical conditions affect floc formation, which is strongly related to coagulation-flocculation treatment efficiency. We explored operational conditions for treatability using metallic coagulants as well as a natural one and supported this fact by displaying different outputs in turbidity removal.

Taking closer attention to floc development assessed by particle size distribution (PSD) through time as a parameter, we indicated that such analysis does not provide a clear picture of the flocculation process. We believe there are inherent limitations to intrusive methods as in *ex situ* dynamic light scattering (DLS), as well as the point that most macroflocs are neglected within this test.

A Visibility Graph (VG) approach allowed insight onto the PSD time series considering the DLS test, but due to the aforementioned limitations, most inferences could not be scaled up to the treatability aspect. In addition, the small number of data points hindered interpretations on the series patterns. However, this does not exclude VG as a promising technique within the environmental and sanitation context but encourages further research on applying network analysis for regular and large time series.

References

Adesina OA, Abdulkareem F, Yusuff AS, et al (2019) Response surface methodology approach to optimization of process parameter for coagulation process of surface water using *Moringa oleifera* seed. South African J Chem Eng 28:46–51. https://doi.org/10.1016/j.sajce.2019.02.002

Adlan MN, Palaniandy P, Aziz HA (2011) Optimization of coagulation and dissolved air flotation (DAF) treatment of semi-aerobic landfill leachate using response surface methodology (RSM).

Desalination 277:74–82. https://doi.org/10.1016/j.desal.2011.04.006

Ahmadlou M, Adeli H, Adeli A (2010) New diagnostic EEG markers of the Alzheimer's disease using visibility graph. J Neural Transm 117:1099–1109. https://doi.org/10.1007/s00702-010-0450-3

Bratby J (2016) Coagulation and flocculation in water and wastewater treatment, 3th edn. IWA Publishing, London

Chen W, Zheng H, Teng H, et al (2015) Enhanced coagulation-flocculation performance of iron-based coagulants: Effects of PO 43- and SiO 32- modifiers. PLoS One 10:1–20. https://doi.org/10.1371/journal.pone.0137116

Ching HW, Tanaka TS, Elimelech M (1994) Dynamics of coagulation of kaolin particles with ferric chloride. Water Res. https://doi.org/10.1016/0043-1354(94)90007-8

de Oliveira AL, Moreno P, da Silva PAG, et al (2016) Effects of the fractal structure and size distribution of flocs on the removal of particulate matter. Desalin Water Treat 57:16721–16732. https://doi.org/10.1080/19443994.2015.1081833

Donner R V., Donges JF (2012) Visibility graph analysis of geophysical time series: Potentials and possible pitfalls. Acta Geophys. https://doi.org/10.2478/s11600-012-0032-x

El foulani A-A, Jamal-eddine J, Lekhlif B (2020) Removal of the colloidal suspension from dam water using mineral coagulants prepared by co-precipitation. Water, Air, Soil Pollut 231:531. https://doi.org/10.1007/s11270-020-04897-0

Elimelech M, Jia X, Gregory J, Williams R (1998) Particle Deposition and Aggregation: Measurement, Modelling and Simulation, 1st edn. Butterworth-Heinemann

Farrow J, Warren L (1993) Measurement of the size of aggregates in suspension. In: Dobias B (ed) Coagulation and Flocculation—Theory and Applications. Marcel Dekker Inc, New York, NY, pp 391–426

Frey DD, Engelhardt F, Greitzer EM (2003) A role for “one-factor-at-a-time” experimentation in parameter design. Res Eng Des 14:65–74. https://doi.org/10.1007/s00163-002-0026-9

Gao Z-K, Cai Q, Yang Y-X, et al (2017) Visibility Graph from adaptive optimal kernel time-frequency representation for classification of epileptiform EEG. Int J Neural Syst 27:1750005. https://doi.org/10.1142/S0129065717500058

Gao Z-K, Cai Q, Yang Y-X, et al (2016) Multiscale limited penetrable horizontal visibility graph for analyzing nonlinear time series. Sci Rep 6:35622. https://doi.org/10.1038/srep35622

Ghafari S, Aziz HA, Isa MH, Zinatizadeh AA (2009) Application of response surface methodology (RSM) to optimize coagulation-flocculation treatment of leachate using poly-aluminum chloride (PAC) and alum. J Hazard Mater 163:650–656. https://doi.org/10.1016/j.jhazmat.2008.07.090

Gonçalves BA, Carpi L, Rosso OA, et al (2019) Quantifying instabilities in Financial Markets. Phys A Stat Mech its Appl 525:606–615. https://doi.org/10.1016/j.physa.2019.03.029

Gonçalves BA, Carpi L, Rosso OA, Ravetti MG (2016) Time series characterization via horizontal visibility graph and Information Theory. Phys A Stat Mech its Appl. https://doi.org/10.1016/j.physa.2016.07.063

Gregory J (2009) Optical monitoring of particle aggregates. J Environ Sci 21:2–7. https://doi.org/10.1016/S1001-0742(09)60002-4

Gregory J, Dupont V (2001) Properties of flocs produced by water treatment coagulants. In: Water Science and Technology

Hammer Ø, Harper DA, Ryan PD (2001) PAST: paleontological statistics software package for education and data analysis. Palaeontol Electron 4:

Iacobello G, Scarsoglio S, Ridolfi L (2018) Visibility graph analysis of wall turbulence time-series. Phys Lett A 382:1–11. https://doi.org/10.1016/j.physleta.2017.10.027

Jarvis P, Jefferson B, Gregory J, Parsons SA (2005) A review of floc strength and breakage. Water Res 39:3121–3137. https://doi.org/10.1016/j.watres.2005.05.022

Jiang S, Bian C, Ning X, Ma QDY (2013) Visibility graph analysis on heartbeat dynamics of meditation training. Appl Phys Lett. https://doi.org/10.1063/1.4812645

Jiang W, Wei B, Zhan J, et al (2016) A visibility graph power averaging aggregation operator: A methodology based on network analysis. Comput Ind Eng. https://doi.org/10.1016/j.cie.2016.09.009

Lacasa L, Luque B, Ballesteros F, et al (2008) From time series to complex networks: The visibility graph. Proc Natl Acad Sci 105:4972–4975. https://doi.org/10.1073/pnas.0709247105

Lacasa L, Luque B, Luque J, Nuño JC (2009) The visibility graph: A new method for estimating the Hurst exponent of fractional Brownian motion. EPL (Europhysics Lett 86:30001. https://doi.org/10.1209/0295-5075/86/30001

Land TMS, Veit MT, da Cunha Gonçalves G, et al (2020) Evaluation of a coagulation/flocculation process as the primary treatment of fish processing industry wastewater. Water, Air, Soil Pollut 231:452. https://doi.org/10.1007/s11270-020-04811-8

Liu C, Zhou WX, Yuan WK (2010) Statistical properties of visibility graph of energy dissipation rates in three-dimensional fully developed turbulence. Phys A Stat Mech its Appl. https://doi.org/10.1016/j.physa.2010.02.043

Long Y (2013) Visibility graph network analysis of gold price time series. Phys A Stat Mech its Appl 392:3374–3384. https://doi.org/10.1016/j.physa.2013.03.063

Miller SM, Fugate EJ, Craver VO, et al (2008) Toward understanding the efficacy and mechanism of Opuntia spp. as a natural coagulant for potential application in water treatment. Environ Sci Technol 42:4274–4279. https://doi.org/10.1021/es7025054

Moruzzi RB, de Oliveira AL, da Conceição FT, et al (2017) Fractal dimension of large aggregates under different flocculation conditions. Sci Total Environ 609:807–814. https://doi.org/10.1016/j.scitotenv.2017.07.194

Muruganandam L, Kumar MPS, Jena A, et al (2017) Treatment of waste water by coagulation and flocculation using biomaterials. In: IOP Conference Series: Materials Science and Engineering

Sacchi GD, Leite L de S, Reali MAP, et al (2020) coagulation and microfiltration application for sugarcane vinasse clarification. Water, Air, Soil Pollut 231:571. https://doi.org/10.1007/s11270-020-04944-w

Saritha V, Srinivas N, Srikanth Vuppala N V. (2017) Analysis and optimization of coagulation and flocculation process. Appl Water Sci. https://doi.org/10.1007/s13201-014-0262-y

Sayama H (2015) Introduction to the Modeling and Analysis of Complex Systems. Open SUNY Textbooks, Milne Library

Shilpa BS, Akanksha, Kavita, Girish P (2012) Evaluation of cactus and hyacinth bean peels as natural coagulants. Int J Chem Environ Eng 3:187–191

Soros A, Amburgey JE, Stauber CE, et al (2019) Turbidity reduction in drinking water by coagulation-flocculation with chitosan polymers. J Water Health 17:204–218. https://doi.org/10.2166/wh.2019.114

Souza Freitas BL, Sabogal-Paz LP (2019) Pretreatment using *Opuntia cochenillifera* followed by household slow sand filters: technological alternatives for supplying isolated communities. Environ Technol (United Kingdom) 0:1–12. https://doi.org/10.1080/09593330.2019.1582700

Subramonian W, Wu TY, Chai S-P (2014) A comprehensive study on coagulant performance and floc characterization of natural *Cassia obtusifolia* seed gum in treatment of raw pulp and paper mill effluent. Ind Crops Prod 61:317–324. https://doi.org/10.1016/j.indcrop.2014.06.055

Supriya S, Siuly S, Wang H, et al (2016) Weighted Visibility Graph with complex network features

in the detection of epilepsy. IEEE Access. https://doi.org/10.1109/ACCESS.2016.2612242

Telesca L, Lovallo M (2012) Analysis of seismic sequences by using the method of visibility graph. EPL. https://doi.org/10.1209/0295-5075/97/50002

Tonhato Junior A, Hasan SDM, Sebastien NY (2019) Optimization of coagulation/flocculation treatment of brewery wastewater employing organic flocculant based of vegetable tannin. Water, Air, Soil Pollut 230:202. https://doi.org/10.1007/s11270-019-4251-5

Wang D, Tang H, Cao F (2000) Particle speciation analysis of inorganic polymer flocculants: an examination by photon correlation spectroscopy. Colloids Surfaces A Physicochem Eng Asp 166:27–32. https://doi.org/10.1016/S0927-7757(99)00420-3

Wang N, Li D, Wang Q (2012) Visibility graph analysis on quarterly macroeconomic series of China based on complex network theory. Phys A Stat Mech its Appl 391:6543–6555. https://doi.org/10.1016/j.physa.2012.07.054

Xiong H, Shang P, Hou F, Ma Y (2019) Visibility graph analysis of temporal irreversibility in sleep electroencephalograms. Nonlinear Dyn. https://doi.org/10.1007/s11071-019-04768-2

Yang Y, Wang J, Yang H, Mang J (2009) Visibility graph approach to exchange rate series. Phys A Stat Mech its Appl 388:4431–4437. https://doi.org/10.1016/j.physa.2009.07.016

Zhu G, Zheng H, Zhang Z, et al (2011) Characterization and coagulation-flocculation behavior of polymeric aluminum ferric sulfate (PAFS). Chem Eng J. https://doi.org/10.1016/j.cej.2011.10.008

Supplementary material

Visibility graph analysis of particle size distribution during flocculation for water treatment

Kamila Jessie Sammarro Silva, Larissa Lopes Lima, Gustavo Santos Nunes, Lyda Patricia Sabogal-Paz*

lysaboga@sc.usp.br*

Fig. S1. Details of the natural coagulant preparation: (a) *Opuntia cochenillifera*; (b) removal of cladodes and spines; (c) cactus cut into pieces; (d) incubator used for drying cacti at 60 °C; (e) aspect of *O. cochenillifera* pieces after 24 hours incubation and; (f) *O. cochenillifera* powder after sieving by 300 μm.

Fig. S2. Flocs formed during flocculation with ferric chloride: (a) view from outside the jartest apparatus; (b) upper view.

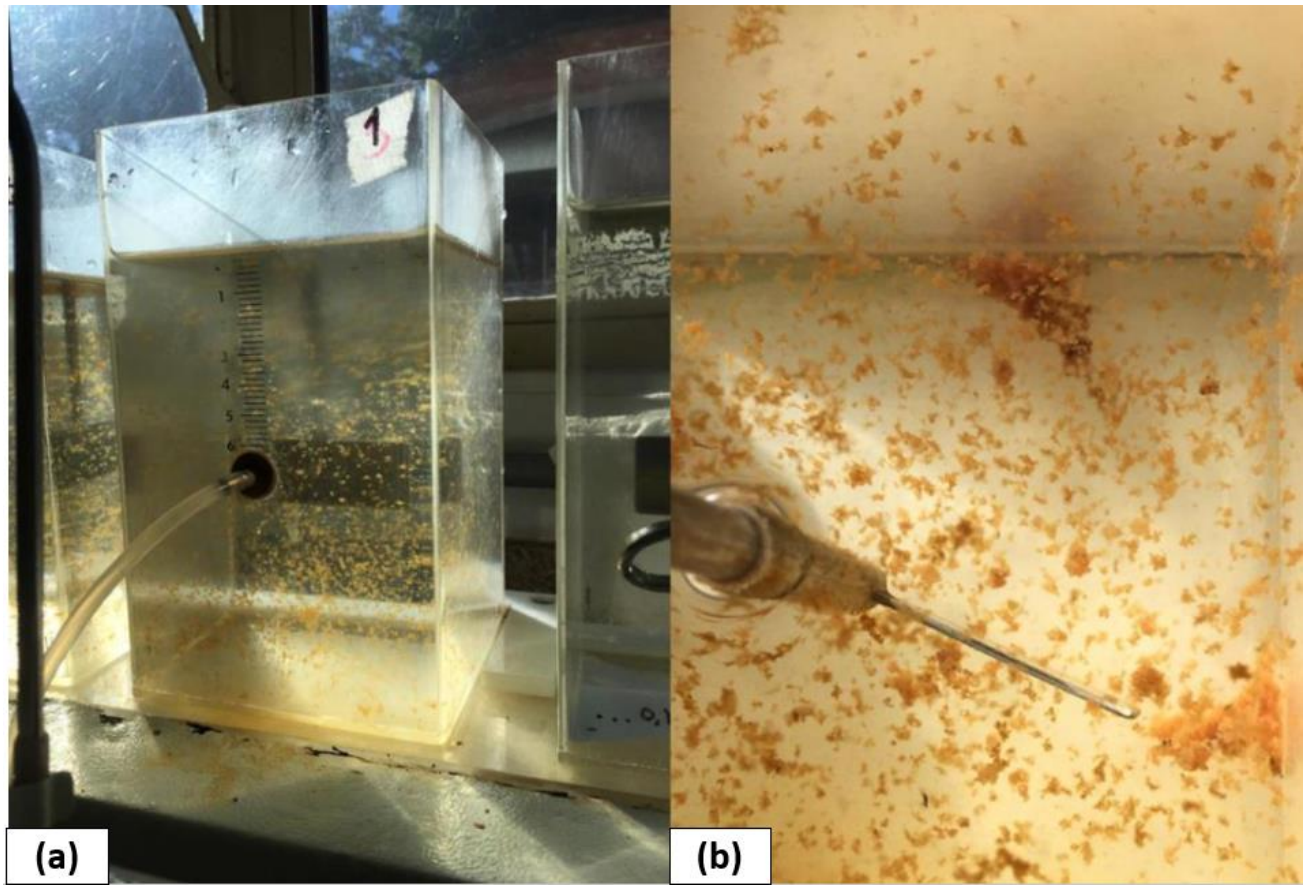

Fig. S3. Flocs formed during flocculation with *O. cochenillifera*: (a) view from outside the jartest apparatus; (b) upper view.